Solid State Phenomena
ISSN: 1662-9779, Vol. 389, pp 37-49
doi:10.4028/p-CeZQ53

Submitted: 2026-01-19
Accepted: 2026-02-16
Online: 2026-04-16

Comparison of PEEK and UHMWPE Cranial Implants Fabricated at Room Temperature Using Single Point Incremental Forming (SPIF)

Mamros Elizabeth[1,a], Clark Austin[2,3,b], Barnett Philip [4,c], Ragai Ihab[2,d*], Shaffer Derek[5,e] and Laser Kristofer Jr.[2,f]

[1]Bucknell University, Lewisburg, PA 17837, USA

[2]The Pennsylvania State University, Erie, PA 16563, USA

[3]GROB Systems Inc., Bluffton, OH 45817, USA

[4]University of Tennessee, Knoxville, TN 37996, USA

[5]Phoenix Laser Solutions, Meadville, PA 16335, USA

[a]elizabeth.mamros@bucknell.edu, [b]aclark@grobsystems.com, [c]pbarnet3@utk.edu, [d*]ihab.ragai@psu.edu, [e]derek.shaffer@phoenixlaser.com, [f]kwl5440@psu.edu

[*]corresponding author

Keywords: incremental forming, PEEK, UHMWPE, cranioplasty, implants, biocompatible, impact testing.

Abstract. The human skull can become fractured or injured through impact and often requires repair through a craniectomy and subsequent cranioplasty, surgery performed to repair defects or damage to the cranium. Challenges related to material choice, which must be biocompatible, and customization for each patient's anatomy remain. One possible solution is fabrication of patient-specific cranial implants, out of biocompatible polymers, using single point incremental forming (SPIF). In this paper, polyetheretherketone (PEEK) and ultra-high molecular weight polyethylene (UHMWPE) are formed using SPIF at room temperature to manufacture a cranial implant. The SPIF process is used to produce formed parts from which test specimens were extracted to evaluate the tensile performance and thermal properties. Formed cranial implants were impacted using a drop weight to evaluate their suitability under relevant conditions. The geometric conformance of the SPIF process was studied to compare the material behavior for the specified polymers after forming. The results validate that SPIF can be conducted at room temperature with PEEK and UHMWPE biocompatible polymers to enable custom implant manufacturing. However, PEEK exhibited superior performance in terms of tensile strength, geometric conformance, energy absorption, and melting temperature, and is recommended over UHMWPE for future implant applications.

Introduction

After sustaining a significant impact to the human head, the brain often swells as part of the body's inflammatory response. In emergency situations, a craniectomy, a surgery that removes a section of the skull to relieve pressure on the brain, may be performed. Later, cranioplasty, a second surgery that repairs the skull by replacing the bone, is performed. The bone is typically replaced by an implant or the patient's own bone. These implants require specific properties and biocompatibility for this application and are often made of commercially-pure titanium. However, challenges, including surface modification required for osteointegration, casting, radiologic incompatibility, and allergy risks [1], have sparked an interest in alternative material options such as polymers.

The use of polymers in biomedical implants offers several advantages, especially in terms of biocompatibility [2], mechanical properties, and design flexibility. Polymers are typically lighter than metals and offer lower heat conductivity. Many polymers, such as polyetheretherketone (PEEK) [3] and ultra-high molecular weight polyethylene (UHMWPE) [4] are bioinert, non-magnetic, radiolucent, and easier to process than metals. More specifically, PEEK is often used due to its similarity to bone in terms of strength and energy absorption properties, which are more similar than titanium. UHMWPE is known for its high wear resistance, high toughness, and low coefficient of

friction. However, it can cause osteolysis, disintegration of bone tissue caused by the introduction of wear particles from an implant.

In recent years, SPIF has increasingly been explored for biomedical applications due to its unique capabilities in forming complex, customized components from sheet materials without the need for dedicated dies. Bagudanch et al. compared forming a cranial implant using UHMWPE and SPIF to a SPIF variant, two point incremental forming (TPIF), which uses a negative die on the non-toolside of the sheet to provide additional support during forming [5]. Chen et al. investigated the temperature-dependent formability of PEEK when fabricating a cranial plate using heat-assisted SPIF [6]. Rosa-Sainz et al. formed cranio-maxillofacial implants using PEEK and SPIF at room temperature to investigate formability [7]. PPS-based composites have been studied for applications of skull repair [8] and orthopedic implants [9], but SPIF of these materials remains unexplored.

In this work, a double dome geometry and a cranial implant were fabricated using SPIF at room temperature and two biocompatible polymers. PEEK and UHMWPE are investigated as potential replacements for titanium in implant manufacturing. Although these materials have been studied separately, a direct comparison is needed to identify the advantages and disadvantages of each of these polymers when fabricating custom cranial implants utilizing SPIF. Material and impact properties, thickness measurements, and geometrical accuracy results are presented.

Materials and Methodology

Materials.

PEEK and UHMWPE were the polymeric materials selected for this investigation. Table 1 shows the associated manufacturing methods.

Table 1. Selected polymeric materials and corresponding manufacturing methods.

Material	Manufacturing Method(s)
PEEK	Injection Molded (IM), Extruded
UHMWPE	Extruded

PEEK.

PEEK samples were injection molded from Victrex 450G pellets at Penn State Behrend. An Arburg 470E 1000-290 was used to make the 152.4 mm × 152.4 mm plaques with a thickness of 3.175 mm. The material was melted in the injection molding barrel set at 416 °C. They were formed at a volumetric fill rate of 111.1 cc/sec. The mold was maintained at 71 °C with the use of a Regloplas P160M steam temperature controller. Prior to molding the material, raw pellets were dried at 149 °C for a minimum of 8 hours. Samples were molded at a 47 second cycle. Additionally, extruded sheets of PEEK, with a thickness of 3.175 mm, were purchased from an industrial supplier.

UHMWPE.

UHMWPE extruded sheets were purchased directly from another industrial supplier with a nominal thickness of 3.175 mm. Sheets were purchased as squares with an initial size of 609.6 mm and were then cut to 152.4 mm squares for the forming process.

Single Point Incremental Forming.

SPIF experiments were conducted using a HAAS vertical 3-axis CNC milling center with consistent parameters for all samples. A hemispherical tool with an 8 mm diameter and free rotation, a feed rate of 2000 mm/min, and a step down size of 0.5 mm were selected based on previous works of the authors [10,11]. An example of the tool is shown in Fig. 1a. All formed sheets had initial dimensions of 152.4 mm × 152.4 mm, and the clamping fixture consisted of two aluminum plates, with a 115 mm (4.5 in) forming area in the center, that were bolted together and held in a Kurt Vice shown in

Fig. 1b. Mastercam [12] was used to generate the toolpath. Experiments that resulted in sample failure were aborted at the first sign of failure. The experimental setup utilized an AMTI MC12-6-4000 dynamometer and Optris 640i infrared (IR) camera for force and temperature measurements, respectively. A thermal image during forming of IM PEEK double dome is shown in Fig. 1c.

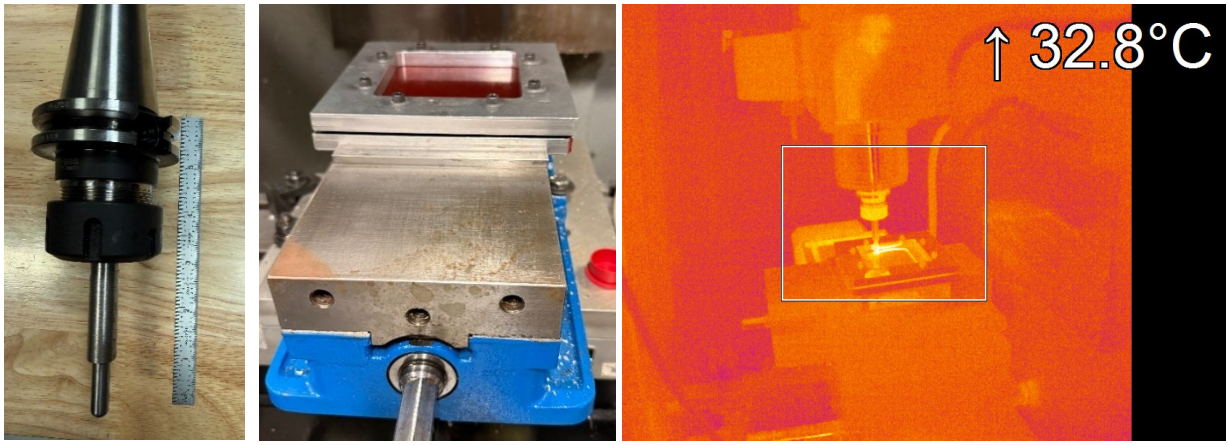

(a) (b) (c)

Fig. 1. (a) Tool geometry, (b) Kurt Vise with fixture setup, and (c) forming set up as seen by the thermal camera.

The geometries of interest were a double dome and a cranial implant as shown in Fig. 2. The double dome geometry, developed for benchmarking a composites formability [13], was intentionally selected to allow for the extraction of tensile specimens from the side walls and flat region. This version represents a modification of the original geometry to account for geometric limitations of the SPIF process. The cranial implant was chosen as a proof of application to the biomedical industry.

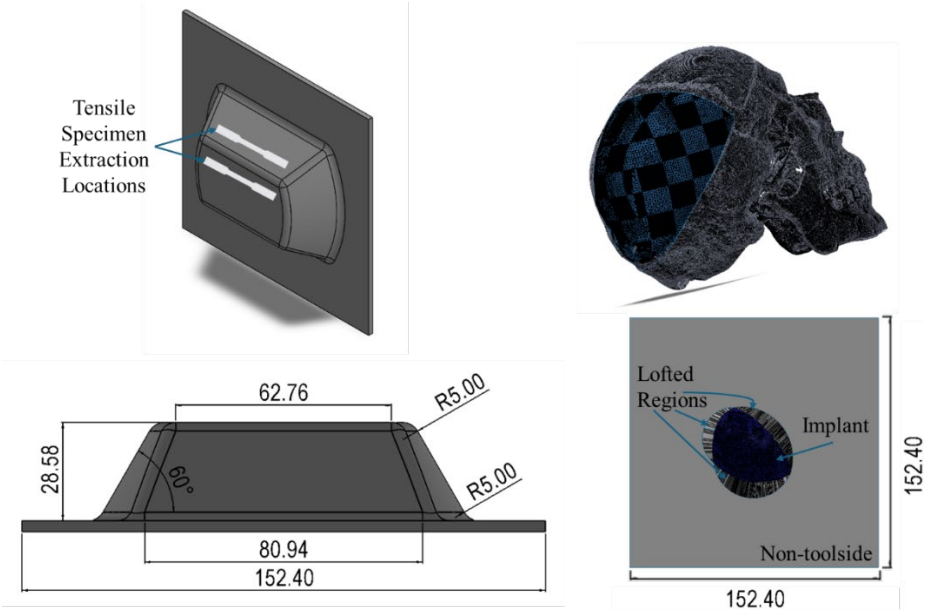

Fig. 2. Target geometries: double dome (left) and cranial implant (right). Units in mm.

Thickness Distribution.

The thickness of the double dome parts was measured using a Magna-Mike 8600 to analyze the material distribution after forming along both principal axes. A total of 15 and 17 thickness measurement points were taken along the major and minor axes, respectively. A magnetic probe is aligned with the desired measurement location on the surface of the specimen, and a metal ball, connected to the probe by a strong magnetic current, is in contact with the opposite surface of the specimen [14]. The distance between the probe and the steel ball constitutes the material thickness at that point. The values were recorded for each specimen at the locations shown in Fig. 3.

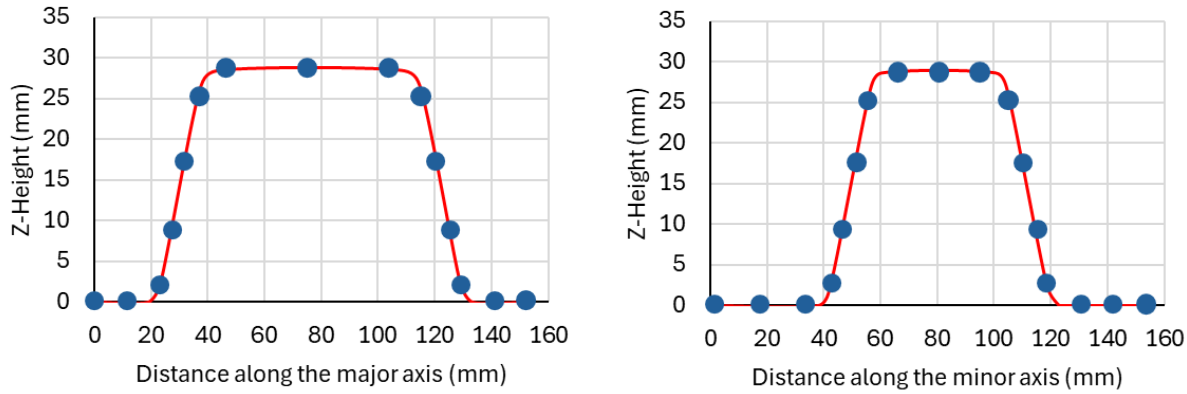

Fig. 3. Double dome measurement locations.

Geometrical Accuracy.

Geometrical accuracy was measured using laser scanning with a Creaform HandySCAN Black Elite as depicted in Fig. 4 which offers up to 0.025 mm of accuracy and is capable of measuring parts from 0.05 m to 4 m in size. The scans were captured using the Creaform OS2 software packaged with mesh resolution settings of 0.5 mm, a shutter speed of 1.55 ms, and a high-resolution scan mode. This provides a high level of dimensional accuracy in the scan while developing a mesh size on the output surface file that is manageable. The three-dimensional models output from these scans were then compared in the Creaform OS2 software to the input CAD models used to generate the SPIF tool paths. In order to do this consistently and align the parts as accurately as possible, the bottom, undeformed regions of the double-domes are used to align the scanned features to the input computer-aided design (CAD) model features. Two-dimensional, cross-sectional overlays are used to visually understand and interpret the data through the center section of the parts. Since the parts are not axisymmetric, two sections are taken perpendicular to each other to fully capture the deviation of the parts. The geometrical accuracy was measured at the same locations as the material thickness for consistency.

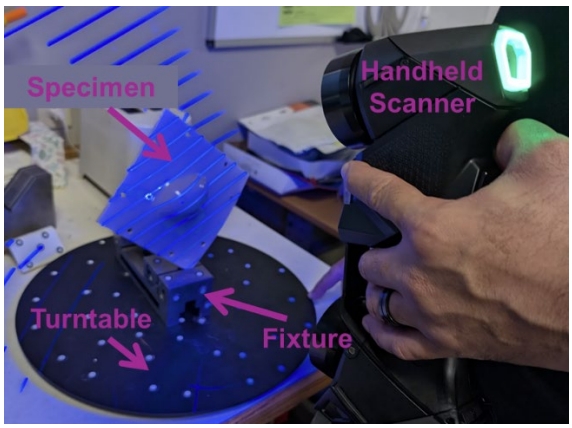

Fig. 4. Handheld scanner experimental setup with scanning targets on the turntable and fixture.

Tensile Testing.

Tensile test specimens were prepared in accordance with ASTM D638 Type V specimens [15]. Waterjet cutting was utilized to extract samples from the modified double-dome geometry in the recessed cavity (representing an unformed region) and the flat portion of the formed walls. Experiments were conducted using an MTS Criterion 43 load frame with a 5 kN cell. The displacement rate was set at 10.0 mm/min (100%/minute strain rate) until specimen failure for each material and manufacturing method. A minimum of three samples were tested for each condition except for the extruded PEEK formed region, for which only one sample was recovered. The tensile modulus, peak stress, and failure engineering strain (i.e., strain at peak stress) are reported in accordance with the test standard.

Falling Dart Impact Testing.

Formed cranial samples were impacted with 278 J of energy from a 20 mm diameter hemispherical indenter with 6.08 kg mass at 9.56 m/s velocity from a 4663 mm drop height (Model 9450, Instron). The force and displacement were measured using a striker instrumented with an internal accelerometer. Specimens were clamped on both sides in a thermostatic chamber as shown in Fig. 5. The temperature was maintained at 37 °C to emulate human body temperature. The system was equipped with an anti-rebound system, which prevents the striker from making multiple impacts with the sample. The impact velocity and energy were chosen to emulate the proposed US National Highway Traffic Safety Administration Federal Motor Vehicle Safety Standard (FMVSS) no. 228 [16], which prescribes a 4.5 kg mass crash dummy head striking a hood or fender at 11.1 m/s (a total of 278 J of energy). It was not possible to achieve the FMVSS recommended mass and velocity combination with the equipment available, so the mass and velocity were matched as closely as possible while maintaining the same total energy.

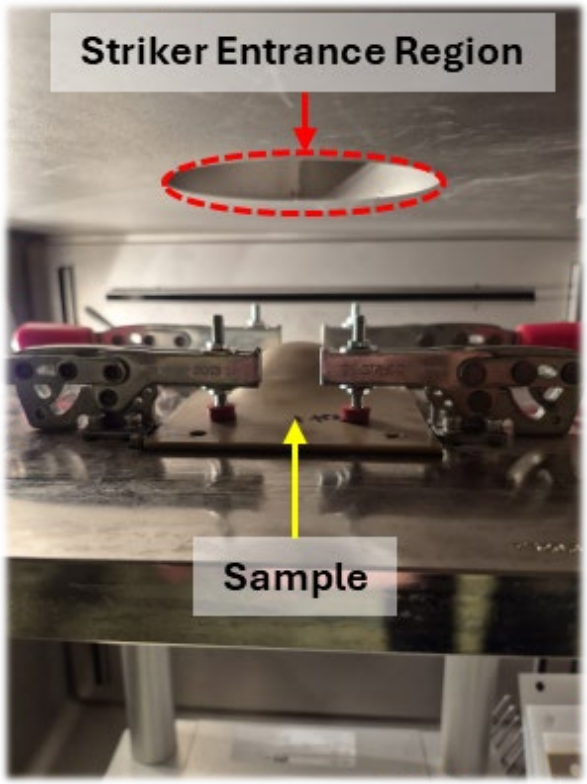

Fig. 5. Inside of thermostatic chamber for impact testing showing the sample clamping mechanism and location of striker impact.

Differential Scanning Calorimetry (DSC).

Samples were extracted from the double-dome formed parts in both the wall and flat regions for thermal analysis. as shown in Samples of 4 mg to 9 mg mass were heated at a ramp rate of 20 °C/min for two cycles (DSC 8500, Perkin Elmer) based on the material: PEEK, 20 °C to 400 °C and UHMWPE, 20 °C to 200 °C. Samples were run in triplicate. The onset and peak melting temperatures were identified from the second cycle, whereas the melting enthalpy was measured from the first to capture the thermal history of the material. The degree of crystallinity, X_C, was determined following equation (1):

$$X_C = \frac{\Delta H_m}{\Delta H_f^0} \tag{1}$$

where ΔH_m is the heat of melting identified from the DSC data and ΔH_f^0 is the enthalpy of fusion for a completely crystalline material (taken as 130 J/g from PEEK and 289.3 J/g for UHMWPE).

Results

Forming Force and Temperature.

Thermal and axial force measurements were collected during the forming process. An example time-temperature distribution plot is shown in Fig. 6a. Temperature data for all tests is shown in Table 2, where Q1 and Q3 represent the first and third quartile measurement values, respectively. In general, PEEK exhibited higher temperatures than UHMWPE in both cranial and double-dome forming while double dome forms yielded higher temperatures than cranial implants due to prolonged forming time. Forming double domes with PEEK exhibited higher temperatures than forming cranial implants with PEEK. However, for UHMWPE, the temperatures during forming double-dome remained comparable to cranial form levels. Additionally, higher axial force on the spindle, that is downward force in the direction of forming (Z-axis), was found in PEEK than in UHMWPE. The X and Y data show oscillations between approximately ±170 N as the tool changes directions during each segment of the toolpath, as show in Fig. 6b. It is hypothesized that the slightly higher negative values indicate that the material exhibits mild anisotropy, which could be addressed in future work. Force data in the direction of forming (Z-axis) is listed in Table 3 and examples of formed implant samples are presented in Fig. 7.

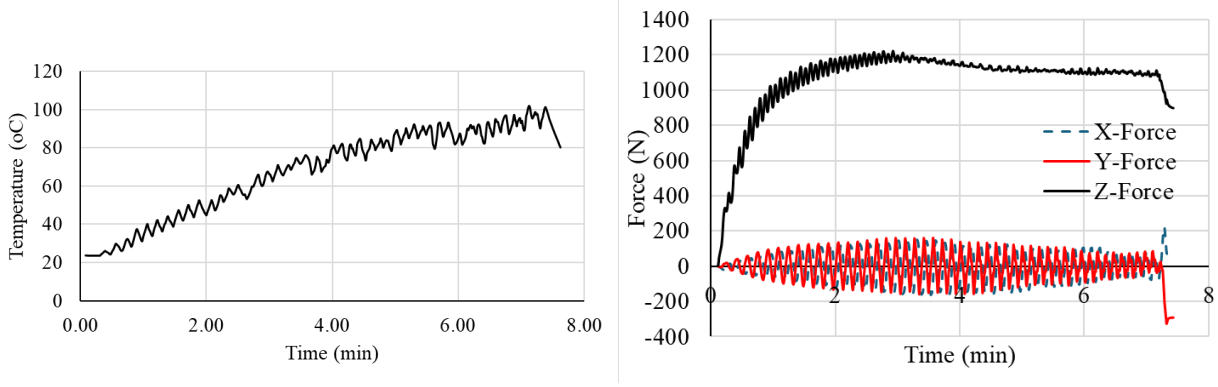

(a) (b)

Fig. 6. (a) IM PEEK Double Dome (a) Time-Temperature distribution and (b) Time-Force distribution.

Table 2. Temperature measurements during forming.

Geometry	Material	Processing	Q1 [°C]	Median [°C]	Q3 [°C]	Maximum [°C]	Std Dev σ [°C]
Cranial	PEEK	Extruded	23.5	27.7	35.2	49.9	7.3
Cranial	PEEK	IM	26.6	35.7	45.5	54.4	10.0
Cranial	UHMWPE	Extruded	23.3	27.8	30.7	34.4	3.9
Double Dome	PEEK	Extruded	51.8	78.1	92.7	112.2	24.3
Double Dome	PEEK	IM	48.9	70.9	85.7	108.3	22.6
Double Dome	UHMWPE	Extruded	29.3	38.4	49.3	56.0	10.5

The force measurements shown in Table 3 represent the first, Q1, and third, Q3, quartile measurement values. The maximum force value recorded occurred during the forming of the cranial implant for the extruded PEEK material. The injection molded PEEK cranial implant required slightly lower (~245 N less) force during forming. In general, the double-dome geometry required lower forming forces than the cranial implant for all three material combinations, with UHMWPE requiring significantly lower forces than PEEK.

Table 3. Axial force measurements (Z-axis) during forming.

Geometry	Material	Processing	Q1 [N]	Median [N]	Q3 [N]	Maximum [N]	Std Dev σ [N]
Cranial	PEEK	Extruded	902.54	1089.81	1255.73	1758.38	387.88
Cranial	PEEK	IM	764.20	945.69	1099.16	1509.73	351.41
Cranial	UHMWPE	Extruded	1117.39	1201.46	1274.42	1592.46	337.18
Double Dome	PEEK	Extruded	1033.32	1115.61	1165.88	1368.27	237.98
Double Dome	PEEK	IM	387.00	541.35	629.87	758.42	189.49

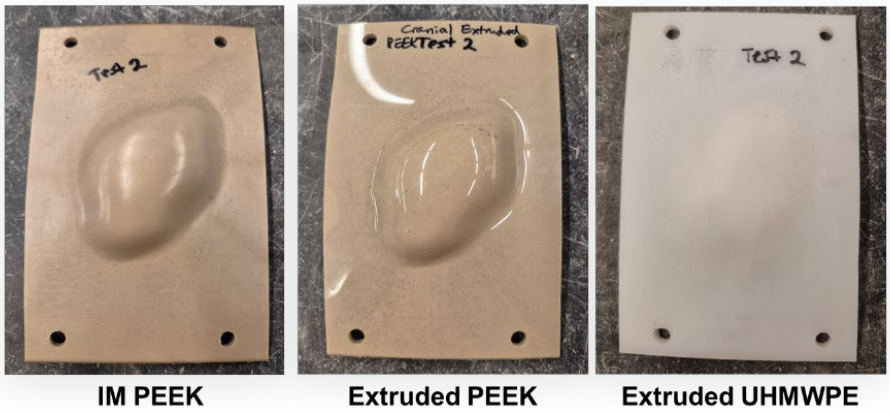

Fig. 7. Examples of formed cranial implant samples.

Thickness Distribution.

Fig. 8 shows that all three materials, formed using the double-dome geometry, exhibit a non-uniform thickness distribution along the distance from the edge of the sheet. Each of these materials exhibits two distinct regions of thinning along the formed walls. In the middle, the thickness distribution represents the undeformed region. The difference in thickness distribution between the three materials can be attributed to the fact that both PEEK and UHMWPE respond differently to temperature. Frictional heat can lead to greater polymer chain lability, especially when near the glass transition temperature, where it thins more readily.

In general, the samples show consistent thinning at high-strain regions (deformed) for all materials. UHMWPE demonstrates superior thickness retention and reduced thinning severity compared to both the extruded PEEK, and IM PEEK. The two PEEK variants exhibit similar forming results, which show that the type of polymer has a stronger influence on thickness distribution than the manufacturing method.

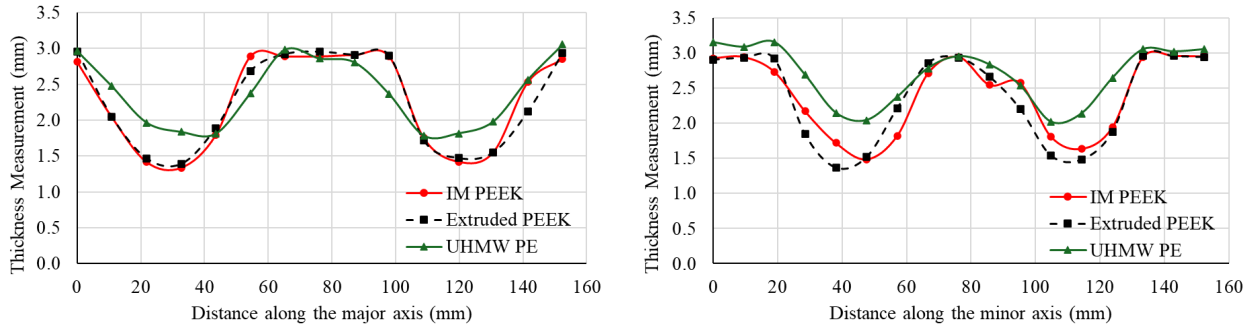

(a) (b)

Fig. 8. Thickness distribution along (a) major axis and (b) minor axis.

Geometrical Accuracy.

Fig. 9 shows the average geometric deviations, with respect to the target geometry CAD model, for two double dome specimens of each material and manufacturing method combination. The geometric deviations were measured at the same locations as the thickness distribution in the previous

subsection. The largest geometric deviations are observed in the flange region for all specimens due to the elastic recovery after removal from the clamping fixture (springback). Towards the center of the geometry, IM PEEK showed the largest geometrical inaccuracy, with the largest positive deviations (~0.11 mm). Contrastingly, extruded PEEK and UHMWPE showed very minimal deviation (~±0.03 mm) in the same region. This indicates that the processing method has a stronger influence on the geometrical accuracy of the formed part than the type of polymer, possibly due to flow-induced anisotropy or residual stress differences due to changing in the cooling rate between the two processing conditions.

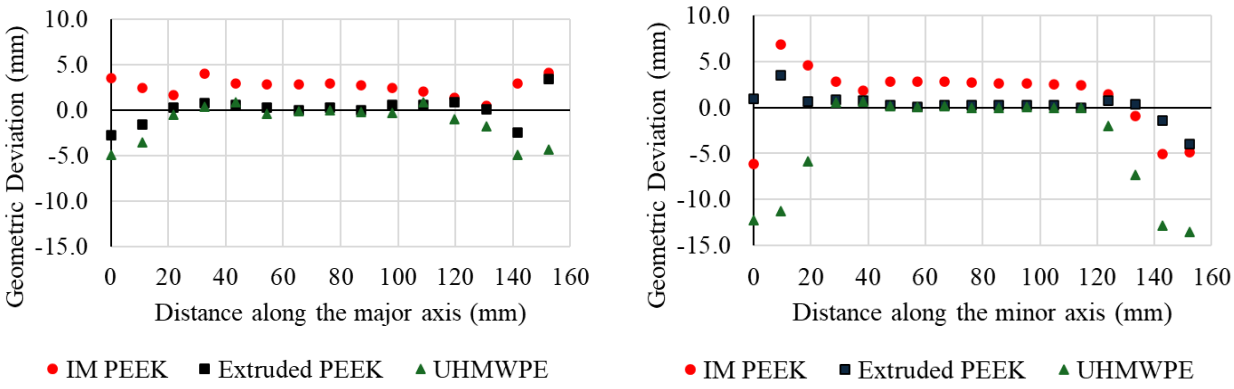

(a) (b)

Fig. 9. Geometric deviation from CAD model along (a) major axis and (b) minor axis.

Mechanical Properties.

The tensile properties of the materials in the formed and unformed regions are reported in Table 4. Specimens extracted from the unformed regions of the PEEK specimens exhibited the same performance for both injection molded and extruded materials. The numbers in parenthesis for the formed regions indicate the p-value in a two-sample student's t-test to identify the statistical significance of the observed changes. This analysis could not be applied to the extruded PEEK samples due to limited sampling; however, the resulting properties were quite similar to the injection molded material. For p-values < 0.05, the properties are statistically indistinguishable between the undeformed and deformed states. The strength and modulus of the PEEK specimens were reduced by 34.8% and 9.4%, respectively. The failure strain had a strong correlation but did not meet the threshold to indicate a statistically significant decrease. This change in performance may be due in part to surface roughness of the formed surface but is also likely the result of molecular chain reorientation during forming. For UHMWPE, the formed and unformed samples were statistically indistinguishable, indicating the forming process had less of an effect on the local mechanical performance.

Table 4. Tensile testing results for specimens extracted from deformed and undeformed regions.

Material	Processing	Region	Strength (MPa)	Modulus (GPa)	Failure Strain (%)
PEEK	IM	Unformed	92.1 ± 0.9	3.2 ± 0.1	6.0 ± 0.2
		Formed	60.1 ± 2.2 (1.41E-9)	2.9 ± 0.2 (0.01)	5.1 ± 1.0 (0.09)
	Extruded	Unformed	94.4 ± 1.8	3.3 ± 0.04	6.0 ± 0.3
		Formed	53.2	2.8	3.6
UHMWPE	Extruded	Unformed	35.3 ± 1.7	1.0 ± 0.05	166.8 ± 5.5
		Formed	35.7 ± 2.9 (0.86)	1.0 ± 0.04 (0.71)	173.4 ± 14.0 (0.48)

During impact testing, the anti-rebound system engaged during the deformation process. This was apparent in the data as a negative force, indicating that the accelerometer had begun accelerating

upward with the engaged system. As such, the energy absorbed was calculated by integrating the force-displacement curve from the point of contact to the first negative force value (Fig. 10). The subsequent data, while still showing an increasing displacement, is no longer physically meaningful (the displacement is simply calculated by double integrating the force signal [17]). Prior to impact, there was a small amount of displacement during the freefall of the impactor, with the force near zero. This region is also excluded from impact energy calculations.

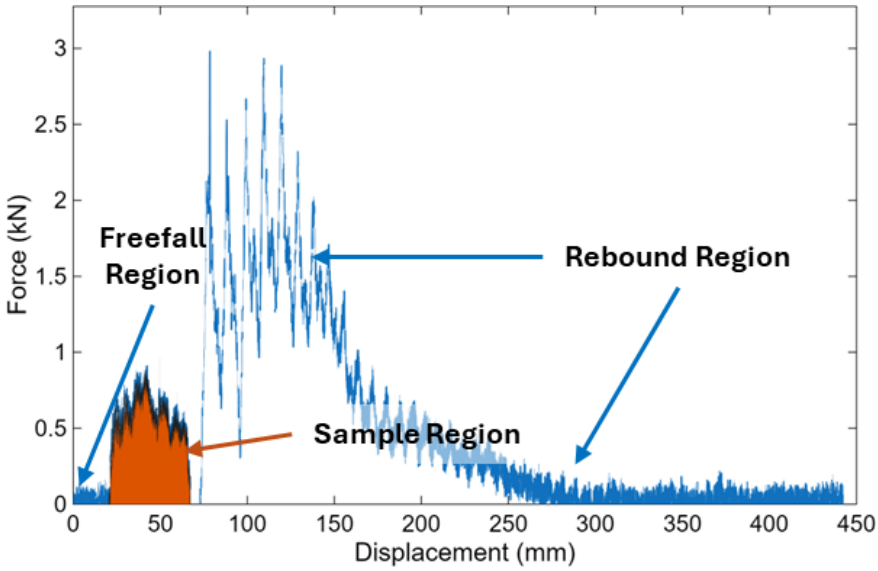

Fig. 10. Example data showing the region of the test data that is integrated to calculate the impact energy absorption of the cranial implants.

Fig. 11 shows the formed cranial implants after the impact. The impact performance of the formed implants is reported in Table 5. For the PEEK specimens, the injection molded material absorbed slightly more energy than the extruded. This is in good agreement with the tensile strength measurements, which showed a slightly higher tensile strength for the extruded PEEK. The reason for these differences requires further study but could be attributed to polymer chain alignment induced during the extrusion process. The UHMWPE absorbed substantially less energy than the PEEK. This is in the range of energy noted to result in skull fracture (14 to 68.5 J [18]). As such, UHMWPE may not be a suitable choice of material for cranial implants, whereas PEEK absorbed substantially more energy than typically required for skull fracture. None of the specimens of either type fractured, instead plastically deforming around the impactor, as shown in Fig. 11.

Table 5. Impact testing results.

Material	Processing	Energy Absorbed (J)
PEEK	Injection Molding	112.2 ± 3.7
	Extruded	126.7 ± 1.9
UHMWPE	Extruded	25.9 ± 0.5

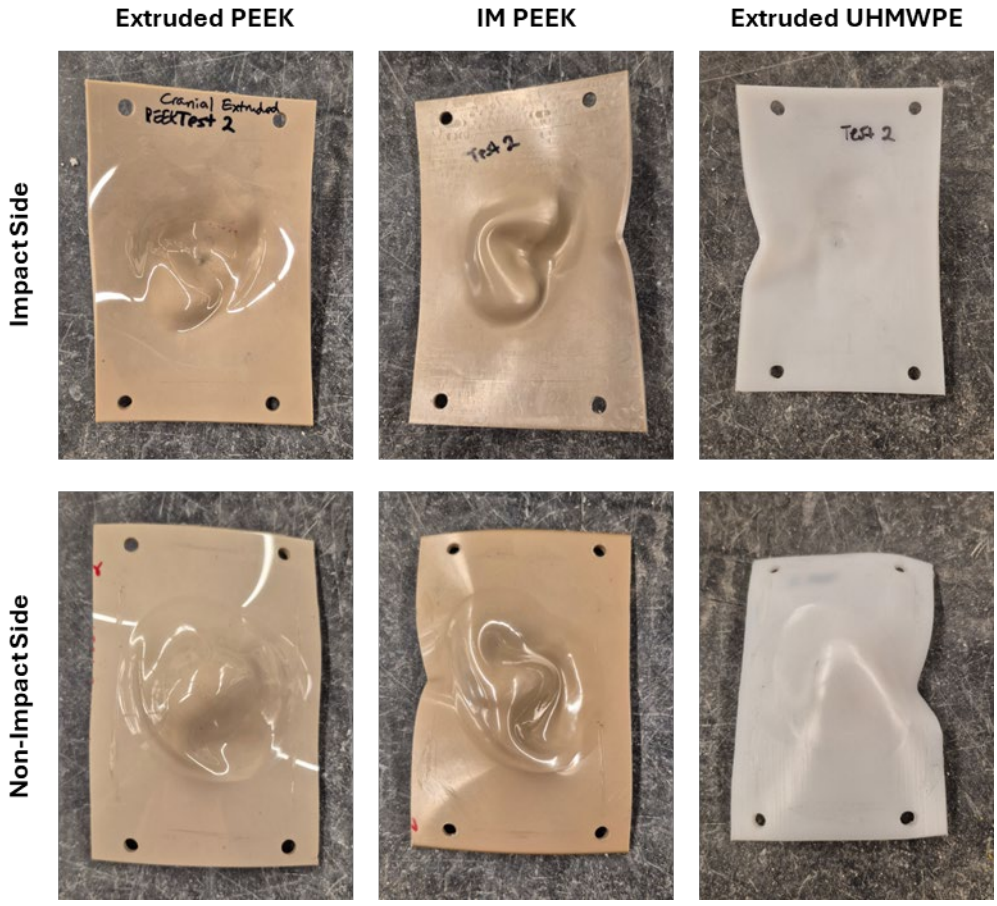

Fig. 11. Typical failure modes for the three materials tested showing no apparent fracture.

Thermal Properties.

The thermal properties of the materials in the formed and unformed regions of the double-dome are reported in Table 6. The injection molded and extruded PEEK were not distinguished in this analysis, but all samples were extracted from the same specimen to ensure repeatability. For the PEEK specimens, the melting onset and peak temperatures did not change substantially due to forming. However, there was an increase in the crystalline percentage, indicating that strain-induced crystallization likely occurred. Several authors have reported evidence of strain-induced crystallization in PEEK, particularly at high strain rates [19,20]. Evaluating the strain rate during the SPIF process is a topic of future work. Alternatively, the increased crystallization may also be due to cold crystallization. During the SPIF process, the temperature rises at the forming locations due to friction between the tool surface and the part, as shown in the IR data.

Table 6. Thermal properties measured using DSC for specimens extracted from formed and unformed regions.

Material	Region	Melting Onset Temperature (°C)	Melting Peak Temperature (°C)	X_C (%)
PEEK	Unformed	327.8 ± 0.9	342.7 ± 1.8	21.9 ± 3.6
	Formed	321.6 ± 6.4	342.7 ± 2.7	25.6 ± 3.4
UHMWPE	Unformed	127.5 ± 0.9	138.8 ± 1.0	48.2 ± 0.2
	Formed	128.8 ± 1.7	139.1 ± 0.9	46.9 ± 1.3

Conclusion

This study investigated the thermal, mechanical, and structural responses of PEEK and UHMWPE during single-point incremental forming (SPIF) of cranial and double-dome geometries. The following points represent the major findings:

- Thermal measurements demonstrated that PEEK consistently reached higher temperatures than UHMWPE, with the highest values observed during double-dome forming due to longer tool–material interaction and increased frictional heating. Force measurements also revealed that PEEK required substantially higher forming forces than UHMWPE, and that cranial geometries imposed greater resistance than double-dome forms.
- Thickness distribution analysis showed that all three materials exhibited non-uniform wall thinning, with characteristic regions of high strain along the formed walls. UHMWPE demonstrated superior thickness retention and reduced thinning severity compared to both extruded and injection-molded PEEK, indicating greater ductility and resistance to localized strain accumulation.
- The geometric deviations measured in the flange region were the largest with respect to the CAD model. Extruded PEEK and UHMWPE showed much greater geometrical accuracy in the center of the double dome geometry along both axes compared to IM PEEK. This indicates that the material processing likely affected the amount of residual stress in the material, which affected the amount of relaxation following forming and unclamping from the fixture.
- The similarity in thickness profiles between extruded and injection-molded PEEK suggests that the polymer type had a greater influence on deformation behavior than initial processing route. Mechanical testing further highlighted that forming significantly reduced the tensile strength and modulus of PEEK, likely due to molecular chain reorientation and surface roughening during deformation, whereas UHMWPE showed no statistically significant change in tensile performance between formed and unformed regions.
- Impact and thermal analyses provided additional insight into the suitability of these materials for cranial implant applications. PEEK exhibited substantially higher impact energy absorption than UHMWPE, exceeding typical skull fracture energy thresholds while retaining structural integrity through plastic deformation rather than fracture.
- Although minor differences were observed between injection-molded and extruded PEEK, both outperformed UHMWPE in terms of energy absorption, which can be critical in preventing reinjury at the implant site.
- Differential scanning calorimetry revealed increased crystallinity in formed PEEK regions, suggesting strain-induced and/or cold crystallization during SPIF, while UHMWPE showed minimal thermal modification.
- Collectively, these results indicate that PEEK offers superior mechanical robustness and impact resistance for cranial implant forming via SPIF, whereas UHMWPE, despite favorable thickness retention, may be less suitable for load-bearing cranial applications due to its lower impact energy absorption capacity.

Acknowledgement

The authors would like to thank James Hart at Phoenix Laser for performing the 3D scans. The authors would also like to thank Mr. Brian Young for injection molding the PEEK specimens, and undergraduate researcher assistants Arame Cisse, Broc Dawson, Senudin Mehinovic, Velia Minerbi, and Mason Sheeley along with Andrew and Christopher Bartlett of Penn State Behrend for their assistance with the experimental work. The authors would like to thank José L. Martínez Collado at the University of Tennessee Knoxville for his assistance in impact testing. We acknowledge the partial support of the US National Science Foundation in the form of a Travel Support Grant [CMMI 2511050], which enabled the authors to attend and present at this conference.

References

[1] Shash, Y. H., 2024, "Cranial Reconstruction Utilizing Polymeric Implants in Two Different Designs: Finite Element Investigation," BMC Musculoskelet Disord, **25**(1), p. 935. https://doi.org/10.1186/s12891-024-08066-w.

[2] Gomes, A. D. S., 2012, *Polymerization*, BoD – Books on Demand.

[3] Toth, J. M., 2019, "Biocompatibility of PEEK Polymers," *PEEK Biomaterials Handbook*, William Andrew Publishing, pp. 107–119. https://doi.org/10.1016/B978-0-12-812524-3.00008-9.

[4] Hussain, M., Naqvi, R. A., Abbas, N., Khan, S. M., Nawaz, S., Hussain, A., Zahra, N., and Khalid, M. W., 2020, "Ultra-High-Molecular-Weight-Polyethylene (UHMWPE) as a Promising Polymer Material for Biomedical Applications: A Concise Review," Polymers (Basel), **12**(2), p. 323. https://doi.org/10.3390/polym12020323.

[5] Bagudanch, I., García-Romeu, M. L., Ferrer, I., and Ciurana, J., 2018, "Customized Cranial Implant Manufactured by Incremental Sheet Forming Using a Biocompatible Polymer," Rapid Prototyping Journal, **24**(1), pp. 120–129. https://doi.org/10.1108/RPJ-06-2016-0089.

[6] Chen, L., Chen, F., Gatea, S., and Ou, H., 2022, "PEEK Based Cranial Reconstruction Using Thermal Assisted Incremental Sheet Forming," Proceedings of the Institution of Mechanical Engineers, Part B: Journal of Engineering Manufacture, **236**(6–7), pp. 997–1004. https://doi.org/10.1177/09544054211045904.

[7] Rosa-Sainz, A., García-Romeu, M. L., Ferrer, I., Silva, M. B., and Centeno, G., 2023, "On the Effective Peek Application for Customized Cranio-Maxillofacial Prostheses: An Experimental Formability Analysis," Journal of Manufacturing Processes, **86**, pp. 66–84. https://doi.org/10.1016/j.jmapro.2022.12.044.

[8] Nie, S., Li, K., Zhou, C., and Sun, J., 2021, "Application and Mechanical Properties of Polyphenylene Sulfide-Based Composite Organic Materials in Skull Repair," Science of Advanced Materials, **13**(1), pp. 55–65. https://doi.org/10.1166/sam.2021.3884.

[9] Deng, Y., Yang, Y., Ma, Y., Fan, K., Yang, W., and Yin, G., 2017, "Nano-Hydroxyapatite Reinforced Polyphenylene Sulfide Biocomposite with Superior Cytocompatibility and in Vivo Osteogenesis as a Novel Orthopedic Implant," RSC Advances, **7**(1), pp. 559–573. https://doi.org/10.1039/C6RA25526D.

[10] Upcraft, C., Diefenderfer, R., Vanderwiel, C., and Ragai, I., 2023, "Toward Better Formability of Polymeric Materials in Single Point Incremental Forming: Effect of Process Parameters," American Society of Mechanical Engineers Digital Collection, New Orleans, Louisiana, USA. https://doi.org/10.1115/IMECE2023-112000.

[11] Mamros, E., Ragai, I., and Young, B., 2025, "Effect of Manufacturing Process on Mechanical Properties of Polyetheretherketone (PEEK) Cranial Implants Produced by Single-Point Incremental Forming (SPIF)," Materials Research Proceedings, **54**, pp. 1191–1200. https://doi.org/10.21741/9781644903599-130.

[12] CNC Software, LLC, "Mastercam." [Online]. Available: https://www.mastercam.com/.

[13] Harrison, P., Gomes, R., and Curado-Correia, N., 2013, "Press Forming a 0/90 Cross-Ply Advanced Thermoplastic Composite Using the Double-Dome Benchmark Geometry," Composites Part A: Applied Science and Manufacturing, **54**, pp. 56–69. https://doi.org/10.1016/j.compositesa.2013.06.014.

[14] "Magna-Mike 8600 Thickness Gauge," Evident Scientific. [Online]. Available: https://ims.evidentscientific.com/en/products/thickness-gauges/magna-mike-8600. [Accessed: 08-Jan-2026].

[15] ASTM International, 2022, “Standard Test Method for Tensile Properties of Plastics.” https://doi.org/10.1520/D0638-22.

[16] National Highway Traffic Safety Administration, 2024, “Federal Motor Vehicle Safety Standards: Pedestrian Head Protection, Global Technical Regulation No. 9.” [Online]. Available: https://www.nhtsa.gov/sites/nhtsa.gov/files/2024-09/NPRM-pedestrian-head-protection-web-version.pdf.

[17] Barnett, P. R., Vigna, L., Martínez-Collado, J. L., Calzolari, A., and Penumadu, D., 2023, “Crashworthiness of Recycled Carbon Fiber Composite Sinusoidal Structures at Dynamic Rates,” Composite Structures, **311**, p. 116847. https://doi.org/10.1016/j.compstruct.2023.116847.

[18] Garcia-Gonzalez, D., Rusinek, A., Jankowiak, T., and Arias, A., 2015, “Mechanical Impact Behavior of Polyether–Ether–Ketone (PEEK),” Composite Structures, **124**, pp. 88–99. https://doi.org/10.1016/j.compstruct.2014.12.061.

[19] “Crystallinity in PEEK and PEK after Mechanical Testing and Its Dependence on Strain Rate and Temperature - Hamdan - 1996 - Journal of Polymer Science Part B: Polymer Physics - Wiley Online Library.” [Online]. Available: https://onlinelibrary.wiley.com/doi/10.1002/(SICI)1099-0488(199603)34:4%3C699::AID-POLB10%3E3.0.CO;2-C. [Accessed: 09-Jan-2026].

[20] “Stages of Structural Ordering Leading to Stress Induced Crystallization of PEEK Films: A Mechano-Optical Study on Deformation, Relaxation and Retraction | Macromolecules.” [Online]. Available: https://pubs.acs.org/doi/10.1021/ma802041n. [Accessed: 09-Jan-2026].